International Journal of Fatigue 148 (2021) 106216

Contents lists available at ScienceDirect

International Journal of Fatigue

journal homepage: www.elsevier.com/locate/ijfatigue

Fatigue resistance of reinforced UHPFRC beams

Bartłomiej Sawicki *, Eugen Brühwiler

Laboratory of Maintenance and Safety of Structures, Structural Engineering Institute, Swiss Federal Institute of Technology (EPFL), Lausanne, Switzerland

ARTICLE INFO

Keywords:
UHPFRC
Full-scale
Testing
Rebar
Cementitious composite

ABSTRACT

This work investigates the fatigue resistance of reinforced Ultra High Performance Fiber Reinforced Cementitious composite (R-UHPFRC) beams with special consideration of steel rebar – UHPFRC interaction under tensile stresses due to bending. Experimental testing of full-scale beams reveals that the fatigue resistance depends on both minimum and maximum loadings in the cycle. The increase of stress range in the rebar during the fatigue process is discussed and quantified. Finally, recommendations for fatigue verification of R-UHPFRC beams are given.

1. Introduction

The reduction of CO_2 emissions, as well as energy and raw materials consumption, in the construction sector leads towards high-performance building materials, limiting their quantities necessary for erection of structures. This, in turn, increases the live-load to dead-load ratio, rising the importance of fatigue resistance. One of such materials is UHPFRC (Ultra High Performance Fiber Reinforced Cementitious composite) with rising use around the world.

The UHPFRC response in tension and compression is fundamentally different. Under direct compression, it remains elastic almost until failure. Under direct tension, due to the composite nature of this material, a bi-linear response is observed. It remains elastic until the elastic limit stress f_{Ute} is reached. Then, the distributed microcracking takes place and the quasi-linear strain hardening slope is followed until the tensile strength f_{Utu} is attained. Finally, the gradual softening occurs [1].

Most of research related to the fatigue behavior of UHPFRC was concentrated on its compressive response, while it is the tensile response that is more relevant from the structural point of view [2–7]. Furthermore, the majority of fatigue tests were conducted on small specimens, whilst it can be expected that in reinforced UHPFRC (R-UHPFRC), i.e. steel reinforcement bars implemented in the UHPFRC, the capacity of stress redistribution in the structural element may be significant.

This paper reports on fatigue tests on T-shaped R-UHPFRC beams under four-point bending. The design of the specimen was inspired by the use of UHPFRC in structural applications as beams or unidirectional slabs [2,8]. Special attention is paid to the interaction of steel reinforcement bars and UHPFRC in the tensile stress region of the beam. The main goal was to explore the presence of a Constant Amplitude Fatigue Limit (CAFL) of R-UHPFRC beams with two types of rebars and under various fatigue load levels. With almost 3 m^3 of UHPFRC casted for specimen fabrication, this research seems to be the most exhaustive experimental campaign on fatigue of R-UHPFRC realized hitherto.

2. Fatigue of UHPFRC and R-UHPFRC

2.1. Overview

Although UHPFRC is a relatively new structural material, there have been already several experimental campaigns on its fatigue resistance reported. The majority of experimental investigations on the fatigue behavior of UHPFRC and R-UHPFRC utilized relatively small specimens, i.e. they were conducted on the material level rather than on the structural level. As far as this kind of testing is crucial for understanding the fatigue process, it does not allow for observation of stress redistribution capacity and rebar-UHPFRC interaction. Therefore, some tests were executed on full-scale structural elements as well. The run-out limits at which the test was stopped and considered as no failure were varying from 1 to 20 million. Taking into account that some of the reported failures occurred after 1 or 2 million of cycles, it can be stated that for many campaigns the runout limit was not enough to identify CAFL of UHPFRC properly, as some of run-outs would have failed soon after the test was stopped. The CAFL is a fatigue loading level that, if fatigue stresses remain below this level, no continuous fatigue damage is produced in the material. Thus, the fatigue duration of a structural element subjected to fatigue loading below the CAFL is considered as

* Corresponding author.
E-mail addresses: bartek.sawicki@epfl.ch (B. Sawicki), eugen.bruehwiler@epfl.ch (E. Brühwiler).

https://doi.org/10.1016/j.ijfatigue.2021.106216
Received 18 October 2020; Received in revised form 1 February 2021; Accepted 20 February 2021
Available online 8 March 2021

infinite.

Furthermore, to obtain fatigue failures after a relatively low number of cycles, considerably high fatigue stresses were applied. Such an elevated fatigue loading, sometimes up to 90% of the static resistance of tested elements, is not realistic, as the requirements of structural safety at the Ultimate Limit State always need to be fulfilled. In addition, no variable stress amplitude testing was performed so far.

To search literature relevant for the current research, the following boundary conditions were set: 1) content of short steel fibers above 2% by volume; 2) largest particle size in the cementitious matrix below 2 mm; 3) at least two fatigue tests conducted in an experimental campaign. It is commonly agreed that the fatigue resistance of UHPFRC depends on the maximum fatigue load level, denoted as S-ratio between the maximum fatigue load and the ultimate static resistance of a given element.

2.2. Axial compressive fatigue tests

The traditional type of fatigue tests on cement-based materials is in uniaxial compression. An extensive testing campaign on different types of high-strength and ultra-high-strength cementitious materials with and without fibers was performed [9] to update the model used in the *fib* Model Code [10]. One of the tested materials was a UHPFRC with maximum grain size of 0.5 mm and 2.5% in volume of straight 9.0 mm long steel fibers of an aspect ratio of 60. It was shown that the CAFL is at 0.6S with respect to a 7 million cycles runout limit.

Another experimental campaign on a UHPFRC (3.8% vol. steel fibers) similar to the one used in the present research was performed by [11]. Plate specimens (30 mm × 100 mm × 450 mm) loaded on the smaller face were tested up to 20 million cycles, and CAFL at 0.6S was confirmed. The shape of specimens was mocking-up the use of UHPFRC in thin-walled elements such as wind turbine towers.

In real structures subjected to fatigue loading, the maximum compressive stress in structural elements rarely reaches half of the compressive strength of UHPFRC [5,7,12]. Additionally, design standards claim for 'ductile' failure modes of structural elements with materials (such as steel) failing in tension.

Consequently, it is considered that the fatigue resistance of R-UHPFRC elements is controlled by the material subjected to tensile stress, similarly to reinforced concrete structures [13–16]. Therefore, the fatigue resistance under compressive fatigue stress is not relevant for structural elements.

2.3. Axial tensile fatigue tests

UHPFRC with 2.5% vol. of steel fibers was tested in direct tension [17] up to 5 million cycles. It was found that the material can withstand fatigue cycles higher than 0.5S. However, for specimens where the maximum stress was above the elastic limit stress f_e, gradual reduction of stiffness occurred even for runouts indicating damaging process and the likelihood of fatigue failure if the tests were continued.

An extensive campaign was conducted by [18], on material with 3.3% vol. steel fibers and runout limits varying between 5 and 20 million. They linked CAFL with the maximum stress applied in the cycle and equal $0.7f_{Ute}$ (0.6S) for material in elastic domain, $0.6f_{Ute}$ (0.5S) when the specimen was pre-loaded to strain-hardening domain and $0.45f_{Ute}$ (0.4S) for specimens pre-loaded to the post-peak softening domain.

The same UHPFRC with incorporated steel reinforcement bars was also tested by [19]. The authors reported that the response of R-UHPFRC subjected to direct tensile fatigue stress comprised three regimes depending on maximum fatigue force F_{max} applied: 1) $F_{max} \leq 0.23S$: both UHPFRC and rebars below the CAFL, 2) $0.23S < F_{max} \leq 0.54S$: UHPFRC above the CAFL, but the stress amplitude in the rebar remains below the CAFL, thus the R-UHPFRC remains below the CAFL, 3) $F_{max} > 0.54S$: both UHPFRC and rebar are above the CAFL, and thus fatigue failure occurs. In the third regime, UHPFRC acts as a stress reducing and distributing agent, increasing the element's fatigue resistance. In the first part of the test, the global deformation was growing when UHPFRC is damaged, then remains almost constant until rebar failure. Only one type of element was tested.

2.4. Bending tests

Numerous fatigue tests on UHPFRC executed under flexure are presented in Table 1. Although for some experimental series a surprisingly high CAFL is found, it can be taken that the CAFL lies at a fatigue loading level of about half of the ultimate static specimen resistance. All reported tests were run under low minimum force level, i.e. $F_{min} < 0.1S$.

Bi-axial bending fatigue resistance was investigated by [27] with ring-on-ring fatigue tests using 50 mm thick circular UHPFRC slabs with a diameter of 1′200 mm. The utilized UHPFRC was the same mix as in [11], with 3.8% vol. steel fibers, and similar to the one used in the present research. The authors have shown that under bi-axial fatigue stress the CAFL is similar as under uniaxial bending, thus 0.54S. Interestingly, this is the load level at which the UHPFRC reaches f_{Utu} on the bottom face of the specimen. This shows that the relative material fatigue resistance is higher in bending than under direct tensile stress which may be due to significant stress redistribution capacity of UHPFRC. The size of the specimen was sufficiently large such that it can be considered as a full-scale test mocking up the real performance of a UHPFRC slab.

2.5. Findings from the literature review

Literature review reveals that most tests have been conducted using small specimens. There were few fatigue tests on structural elements involving UHPFRC [17,28] or R-UHPFRC [29–35]. However, in most experimental campaigns only one or two specimens were tested, not allowing for closer investigation of fatigue damage mechanism and resistance of the element. All of them were run under low minimum force ($F_{min} < 0.1S$) and have shown that CAFL $\geq$ 0.5S.

3. Materials and methods

3.1. Experiment set-up

Three types of beams were tested: Type I with a single Ø20 mm rebar; Type II with a single Ø34 mm rebar and Type III with Ø20 mm rebar and Ø6 mm Ω shaped stirrups (Fig. 1). The beams were casted in horizontal position (as tested), pouring the fresh UHPFRC from top at one end. Six external vibrators were used to assure good flow of the fresh UHPFRC. Each casting comprised three identical beams, two to be tested under fatigue loading and one to be tested under quasi-static loading to determine the ultimate resistance as reference value. In total three castings of Type I, three of Type II and two of Type III were performed.

Table 1
Summary of flexural fatigue tests on UHPFRC.

Reference	Specimen dimensions [mm]	Fiber content [% vol.]	Runout ($\times 10^6$)	CAFL (S)
Four-point bending				
[20]	40 × 200 × 600	11.0	2	0.5
[21]	125 × 125 × 1000	2.5	10	0.55
Three-point bending				
[22]	100 × 100 × 400	2.0	1	>0.5
[23]	35 × 90 × 360	8.0	20	0.85
[23]	100 × 100 × 500	8.0	1	<0.7
[24]	100 × 100 × 400	2.0	5	0.65
Three-point bending notched				
[25]	100 × 100 × 440	2.5	2	0.49
[26]	75 × 75 × 275	2.0	2	0.65

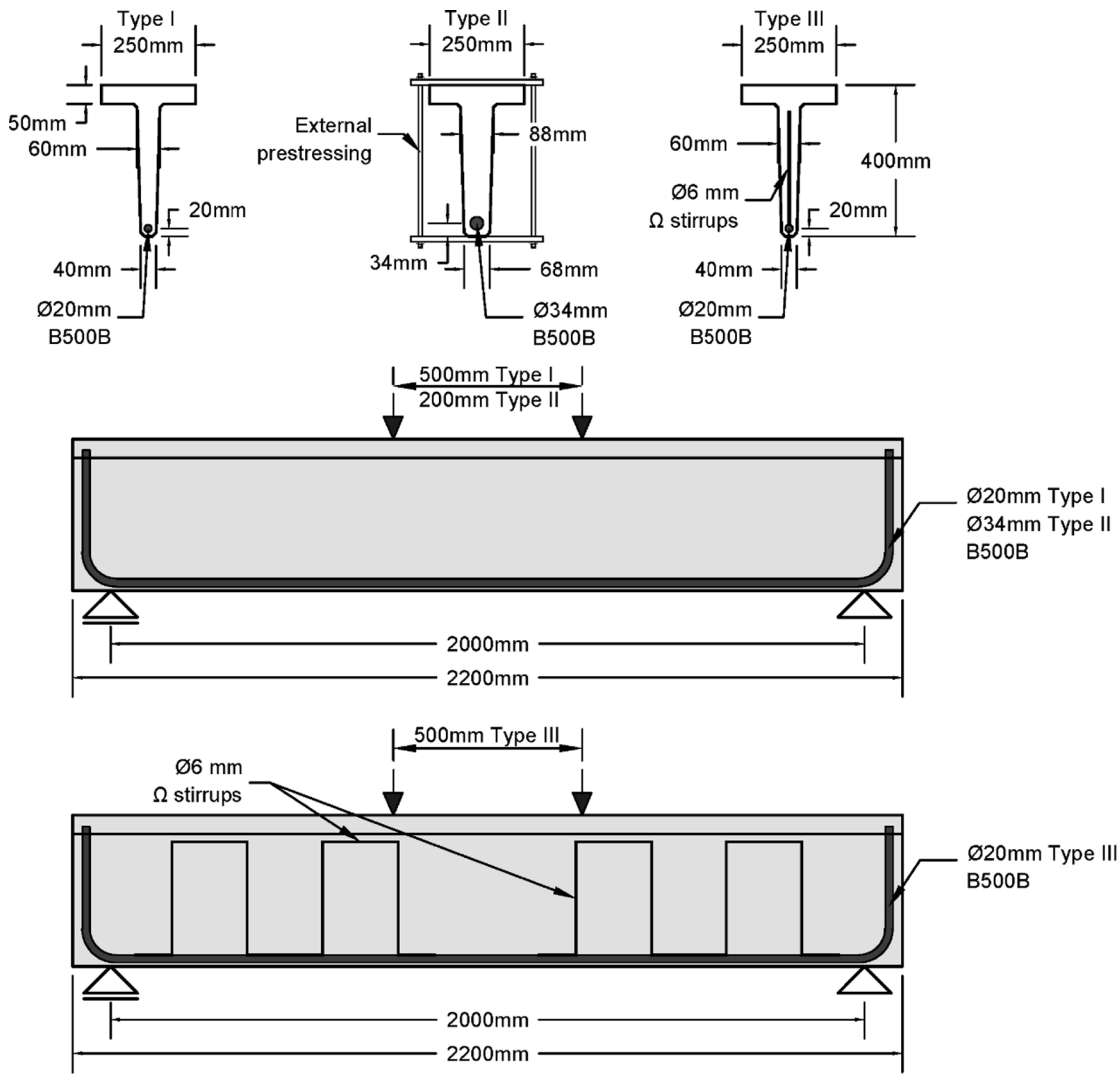

Fig. 1. Scheme of beams under testing.

All beams were tested under four-point bending. Loading was applied using one servo-hydraulic actuator and a steel redistribution beam of high stiffness. The application points were positioned symmetrically at ±250 mm from mid-span for beams Type I and III, and at ±100 mm for Type II. Smaller spacing was adopted for Type II beams to avoid shear failure. For the same reason Type II beams were strengthened using externally mounted posttensioned stirrups (Fig. 1) outside constant bending moment zone. This solution was chosen to limit the size of tested element, instead of increasing the beam span. Furthermore, longer span would increase the beam deflection and thus the actuator's stroke, limiting the frequency of loading cycles and thus increasing the time necessary for testing. Since the beams were tested under four-point bending, the shear strengthening did not affect the bending strength.

All beams were instrumented with extensometers glued on the UHPFRC surface at the level of the axis of reinforcement bar, along the constant bending moment zone. The measurement base was equal to 100 mm, therefore the number of extensometers varied depending on the type of beam: seven for beams Type I and III, four for Type II. The force was measured with the force cell of the actuator. Some of the beams (1–5, 6, 9, 10–11) were equipped with foil strain gauges glued on the rebar before casting. The gauges were glued on top of the rebar after cleaning the surface, in the constant bending moment zone. Thanks to the use of small-sized gauges (6 mm × 2.2 mm) and a protection cover of limited extent, the distortion of stress field in the vicinity of the gauges was minimized.

The testing rig was able to accommodate two beams at the time, reducing the duration of the experimental campaign. Each beam was loaded with a separate actuator, and thus the two tests were conducted independently.

3.2. Materials

Commercially available UHPFRC mix Holcim710® was used, with 3.8% in volume of 13 mm long straight steel fibres with an aspect ratio of 65. The minimum age at the moment of testing was three months. The cement hydration in UHPFRC is largely advanced after 28 days and nearly complete after 90 days. Therefore, the age of testing of the R-UHPFRC beams has no notable influence on the material properties [36]. To confirm this, UHPFRC was tested in four-point bending according to Swiss standard SIA 2052 [12] at the age of 28 and 90 days. The testing was conducted for four castings, leading to eight testing series, with six 30 mm × 100 mm × 500 mm plates for each series. The following properties were determined: 1) elastic limit stress f_{Ute}; 2) tensile strength f_{Utu}; 3) hardening strain at tensile strength ε_{Utu}; and 4) modulus of elasticity E_{Ut}. The average values presented in Table 2 show that after 28 days no significant increase in strength properties is noticed. The average compressive strength was $f_{Uc} = 140$ MPa, tested on cylindrical specimens, 70 mm × 140 mm, at 28 days in accordance to

Table 2
Mean tensile material properties of UHPFRC based on four-point bending tests of plates.

	f_{Ute} [MPa]	f_{Utu} [MPa]	ε_{Utu} [‰]	E_{Ut} [GPa]
28 days	5.50	11.48	3.38	40.01
90 days	5.55	12.00	3.52	41.09
Average	5.52	11.75	3.46	40.59

SIA 2052 [12].

Both longitudinal rebars and stirrups were of type B500B according to [37] and [38], with nominal yielding stress $f_{sk} = 500$ MPa, quenched and self-tempered. The properties of the longitudinal reinforcement bars were obtained using direct tension test and are presented in Table 3. The rebars used in Type I beams have higher strength. However, they still conform to the requirements of B500B reinforcement bar class. Due to large differences in strength values of reinforcement bars, Type I and III beams are treated separately.

3.3. Test description

In the beginning of each fatigue test, pseudo-static cycles were imposed under displacement control of the actuator. Before reaching the maximum force foreseen for fatigue testing F_{max}, gradual loading was applied. Several unloadings to the minimum testing force F_{min} were executed from increasing force levels to determine the residual strain when UHPFRC enters the strain-hardening domain. This procedure also allows comparing with the reference beam and confirming the same structural behavior and resistance.

After this initial quasi-static part, the actuator was switched to force-control mode, and the fatigue test started. Sinusoidal constant amplitude force was applied with a frequency varying between 3.3 Hz and 4.5 Hz, depending on the response of the testing rig under the applied loading. It may be assumed that frequencies below 10 Hz have no influence on the fatigue resistance of UHPFRC [11,21,39,40]. Testing frequencies higher than 10 Hz can be detrimental for fatigue resistance [41] due to increased temperature of the specimen modifying the viscoelastic behavior and thermal expansion of the cementitious matrix [42]. To guarantee that no such effect takes place, some of the beams were instrumented with thermocouples embedded in UHPFRC before casting, as well as glued on the surface. As no thermal gradient was recorded, it may be assumed that the testing frequency had no influence on the results.

Despite the relatively high frequency of fatigue cycles imposed to the beams, a test could take more than one month. For one of the beams almost 27 million fatigue cycles were reached, which may be the longest-lasting fatigue test on an UHPFRC structural element ever reported, with three months of testing duration.

All three types of beams were subjected to two groups of fatigue loading, with low minimum force ($F_{min} < 0.1S$) and high minimum force ($F_{min} \approx 0.35S$). This range is representative for typical bridge structures.

4. Results

Table 4 presents the results of all fatigue test executed in this study, fourteen beams in total. The runouts, thus beams which did not fail under the imposed fatigue loading until end of the test, are marked with (R) next to the number of cycles. The stress in the reinforcement bar was calculated using UHPFRC properties obtained by means of an inverse analysis of the reference beam, taking into account the loading-unloading behavior due to strain-hardening as described in [43].

Table 3
Mean tensile material properties of reinforcement bars based on axial tensile tests.

Beam type	f_s [MPa]	f_t [MPa]	ε_u [%]
Type I (Ø20 mm)	600	687	9.2
Type II (Ø34 mm)	525	624	9.4
Type III (Ø20 mm)	512	617	9.2

4.1. Global fatigue resistance

Studies by [9,11] have shown that the CAFL of UHPFRC in compression is equal to 60% of ultimate static resistance. In the present beams, this magnitude of stress is reached only at the ultimate bending resistance. Therefore, as expected, all beams failed due to fatigue damage of UHPFRC in the bottom tensile part of the web and fatigue rupture of the reinforcement bar. No UHPFRC cracking or matrix spalling was observed in compressed portion of the member.

According to other authors [19,27,44], the fatigue resistance of UHPFRC depends on the imposed maximum fatigue stress. However, all their tests were executed in the low minimum force domain. To visualize the influence of both maximum and minimum load, the modified Goodman diagram is suitable to present results (Fig. 2). For each fatigue test the normalized mean cyclic load is marked on the abscissa, and both maximum and minimum loads are on the ordinate axes. Failures are marked with an X, runouts with a circle. The fatigue safe region is delimited with two straight dashed lines enclosing the runout tests and crossing in point (1,1) standing for the quasi-static ultimate resistance. Similar approach was used in [45] for reinforcement bars.

The results presented in Fig. 2 show a clear delimitation between fatigue-failure and fatigue-safe domains. All fatigue tests with failure lie within the fatigue failure domain. Only Test 10 is a runout which theoretically should have failed. However, after a slight increase of F_{max}, the beam (Test 10A) failed after relatively few fatigue cycles. The scatter of results is rather limited for fatigue tests. This shows that the assumption of the fatigue safe domain is realistic. Interestingly, Test 14 was subjected to over 26 million fatigue cycles and showed no failure. After load increase into the fatigue failure domain, Test 14 specimen failed after 1 million cycles (Test 14A). Importantly, no dependence of the failure location or fatigue resistance of the beam on the presence of strain gauge on rebar was identified. Most probably, it is because of the very good bond between UHPFRC and reinforcement bar [46] and small size of the gauge.

For the sake of comparison, the validity zone of fatigue design provisions for R-UHPFRC members in [12] is presented as shaded area. The standard suggests global fatigue verification on the member level with the CAFL in bending being equal to half of the ultimate static resistance. This relation is valid up to $F_{max} = 0.5S$ if minimum force is close to zero.

All test results follow the same trend, irrespective of type of reinforcement bar, and are consistent thanks to the normalization of the fatigue stress level with respect to the ultimate static resistance. Consequently, the presented modified Goodman diagram is applicable to any kind of R-UHPFRC member.

4.2. Fatigue stress range in the reinforcement bar

According to [19,44] the strain, and therefore stress, in rebars is growing during the first 0.5 million of cycles. The degree of growth is dependent on the reinforcement ratio [44]. Therefore, the strain growth is presented separately for beams with Ø20 mm and Ø34 mm rebars. Under the assumptions of a) perfect bond between UHPFRC and reinforcement bar [46] and b) UHPFRC bulk material being a continuum before reaching ε_{Utu}, the strain increase measured on the surface of UHPFRC is identical with strain increase in the reinforcement bar.

These assumptions are confirmed by direct strain measurements on the reinforcement bar using strain gauges. In Fig. 3, the strain ranges measured for the whole duration of the tests are presented for both failure and runout tests as well as for high and low minimum force levels. The strain range is normalized with respect to the values measured during the 1st cycle ($\Delta\varepsilon_1$) to quantify its increase during the

Table 4
Summary of fatigue tests; runouts are marked with (R); stress levels (σ) and stress ranges (Δσ) refer to the reinforcement bar.

N°	Type	N° of cycles (M)	M_{min} (S)	M_{max} (S)	σ [MPa]	Δσ [MPa]	Stress transfer increase	Increased Δσ [MPa]
1	I	7.8 (R)	0.06	0.53	140–292	152	1.6	243
2	I	15.1 (R)	0.06	0.53	140–292	152	1.6	243
3	I	0.3	0.33	0.81	298–497	199	1.35	269
4	I	1.1	0.33	0.68	262–390	128	1.35	173
5	I	0.4	0.03	0.53	150–313	163	1.6	261
6	II	8.6 (R)	0.04	0.47	65–223	158	1.3	205
7	II	0.3	0.36	0.79	230–460	230	1.1	253
8	II	6.3	0.04	0.53	62–225	163	1.3	212
9	II	0.9	0.04	0.53	62–225	163	1.3	212
10	II	10.0 (R)	0.36	0.71	233–365	132	1.1	145
10A		1.0	0.36	0.77	245–416	171	1.1	188
11	II	1.8	0.37	0.77	261–416	155	1.1	171
12	III	2.4	0.05	0.56	131–283	152	1.6	243
13	III	0.8	0.33	0.79	285–436	151	1.35	204
14	III	26.0 (R)	0.09	0.53	131–262	131	1.6	210
14A		0.8	0.09	0.59	161–319	158	1.6	253

whole test duration. The number of cycles is normalized with respect to the total number of cycles. Also, the Young's modulus of steel rebars is assumed to remain constant during the fatigue test. The strain range increases quickly during the first part of the test and remain stable for most of the time i.e., in the range from 0.1 to 0.9 of normalized cycles' number. The strain range is fatigue-relevant during this stable part, therefore should be taken into account during fatigue resistance verification of rebars.

The strain range increase measured for beams of Type I (Ø20 mm rebars) and Type II (Ø34 mm) are presented in Fig. 3. For all tests, the growth measured with extensometers is similar to, or larger than, the one measured with strain gauges. This may be explained either by a transverse strain gradient in the beam or by the fact that extensometers cover a much larger area of the beam while strain gauges are installed locally. Therefore, not all the regions with increased strain can be identified using strain gauges. Consequently, the values obtained with extensometers should be taken as representative for the constant bending moment zone. The increase of strain range for both failure and runout tests is similar. For beams with $F_{min} < 0.1S$, the rise is higher than for beams on high minimum force levels. This may be due to stress redistribution and additional microcracking of UHPFRC. For highly stressed beams, this microcracking is already well developed after the 1st loading cycle, and consequently, there is a rather low energy dissipation capacity.

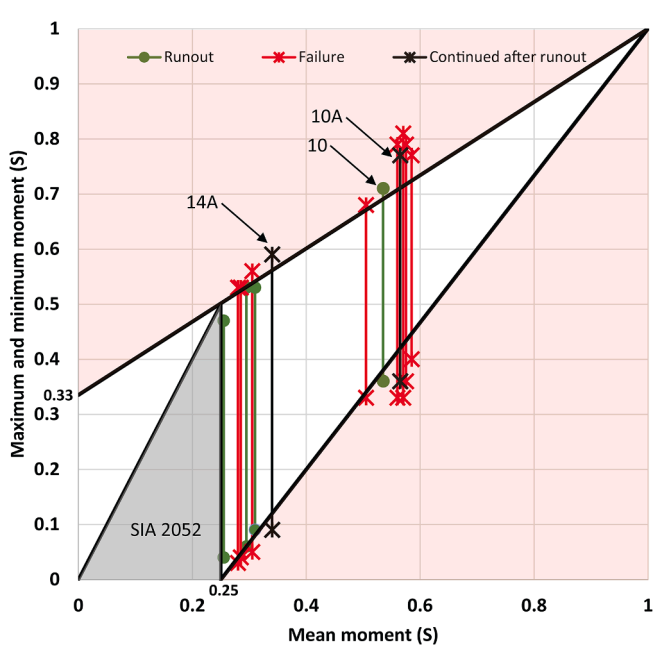

Fig. 2. Modified Goodman diagram showing all fatigue tests results.

The decrease of strain range measured with one of the extensometers in Test 4 (Fig. 3b)) is probably due to rapid deterioration of UHPFRC nearby. This led to local unloading of the material and thus decrease of strain measured by the neighboring extensometer. Importantly, despite this weakening observed, this beam survived more than 1 million fatigue cycles confirming significant redistribution capacity of UHPFRC.

From the above, it can be deduced that the maximum rise of stress range in the rebar due to fatigue of UHPFRC is equal to:

- 60% (1.6 of strain range in 1st cycle $\Delta\varepsilon_1$) for Ø20 mm bar and 30% (1.3 $\Delta\varepsilon_1$) for Ø34 mm bar for the tests with low minimum fatigue force level ($F_{min} < 0.1S$), and
- 35% (1.35 $\Delta\varepsilon_1$) for Ø20 mm bar and 10% (1.1 $\Delta\varepsilon_1$) for Ø34 mm bar for the tests with high minimum fatigue force level ($F_{min} \approx 0.35S$).

For both rebar diameters, the ratio of strain range increase between low and high minimum force level tests is the same. This ratio is equal to 1.18 (1.6/1.35 = 1.3/1.1 = 1.18), thus proportional to F_{min}, irrespective of beam type.

[44] stated that the increase of stress range in rebars is inversely proportional to reinforcement ratio of element. In the present study, this simple rule was not confirmed. The ratio of stress range increase for Ø20 mm and Ø34 mm rebar is 23% (1.6/1.3 = 1.35/1.1 = 1.23) while the proportion of the two reinforcement ratios is 43% (1.0%/2.3%=0.43), and 1/0.43 = 2.33. Therefore, the present test results do not allow to define a relationship between reinforcement ratio and increase in stress range in rebar.

The obtained factors were used to calculate the acting stress range in the rebar, based on the stress range in the first cycle obtained with the inverse analysis method, as given in Table 1. The stress ranges in rebars calculated in this way are presented in Fig. 4 on the S-N curves for Quenched and Self-Tempered (QST) rebars provided by [47]. Tests that do not follow closely the results from the previous study are presented with their respective test numbers.

Fig. 4 reveals that all tests which do not comply with results presented by [47] ended with premature failure. If the fatigue verification of these beams had been performed only regarding stress range in rebars, unexpected structural failures would occur. This demonstrates importance of two-level fatigue verification including the global fatigue resistance check with the modified Goodman diagram.

Test 8 with fatigue failure, should have been a run-out test according to the S-N curves for rebars. This beam failed after more than 6 million cycles, while the runout limit adopted for rebar diameter larger than 20

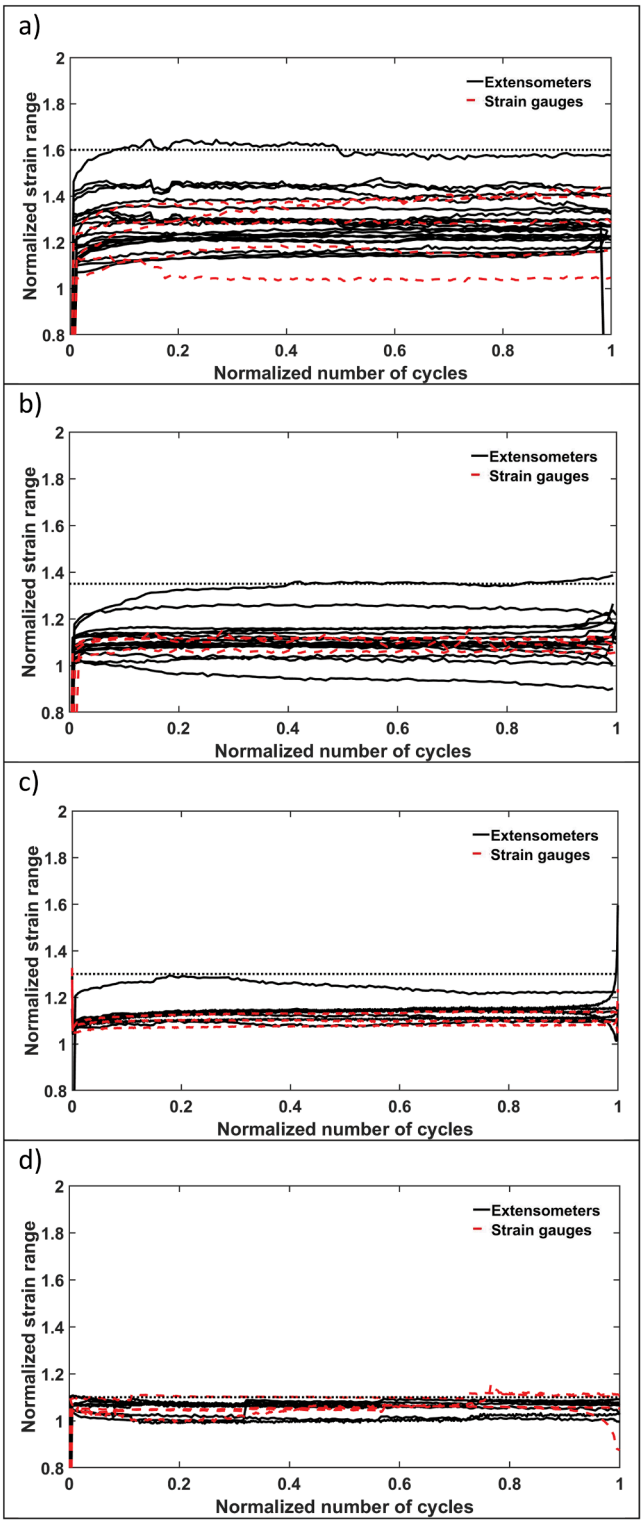

Fig. 3. Normalized strain range variation during the fatigue test: a) Type I beams, $F_{min} < 0.1S$ (Tests 1, 2 and 5); b) Type I, $F_{min} \approx 0.35S$ (3,4); c) Type II, $F_{min} < 0.1S$ (6,9); d) Type II, $F_{min} \approx 0.35S$ (10,11).

mm was 5 million cycles. Thus, this test would have been classified as a runout.

Test 9 failed much earlier (0.9 M) under same loading indicating that the scatter in R-UHPFRC beams could be higher than for rebars tested alone. This may be explained by stress localization resulting from non-uniform microcracking or localized fatigue damage of the UHPFRC.

Test 5 is the only test with low minimum fatigue stress level that failed earlier than expected when considering the stress range in the rebar. The applied loading range was $\Delta M = 0.5S$, therefore it would comply with the fatigue provision in [12], while it is just outside the no failure criterion using the proposed modified Goodman diagram (Fig. 2). This shows again that both maximum and minimum fatigue load levels need to be considered in fatigue design provisions.

All tests with high minimum fatigue load level failed earlier than expected when considering the stress range in the rebar. The stress transfer from the UHPFRC to the rebar is taken into account using the previously determined increment factors. Therefore, the obtained results suggest that the fatigue resistance of contemporary quenched and self-tempered reinforcement bars is dependent not only on the stress range, but also on the minimum stress, similarly to hot-rolled bars [45,48,49].

4.3. Discussion of Test 10

As mentioned previously, Test 10 should have failed according to the modified Goodman diagram given in Fig. 2. That is why it needs to be discussed together with Test 10A and 11 for comparison. Test 11 was subjected to a similar fatigue stress level comparing to Test 10. The beams were casted together and can thus be considered as identical.

The calculated stress profiles in the UHPFRC under maximum and minimum fatigue load in the first cycle are presented in Fig. 5. The stress values were calculated using the material properties obtained from inverse analysis of the reference beam as described in [43]. However, the increase of stress range in the reinforcement bar discussed previously is not taken into account.

At first sight, the stress profiles of all three beams seem to be similar. Importantly, the level below which UHPFRC enters strain softening, i.e. the height at which tensile stress equal to f_{Utu} is reached, is different. In Tests 10A and 11, it lies above the rebar axis, while in Test 10 it is below. As the UHPFRC cover is thin (Ø/2), it can be assumed that the UHPFRC of the very bottom part of the beam is not fully contributing to the global response. Furthermore, the alignment of fibers in this region, due to the small spacing between rebar and formwork, probably leads to locally increased f_{Utu} [50]. Hence, UHPFRC stress in this region is below the tensile strength, contrary to results obtained for the whole beam by inverse analysis. This local variation of stress transfer capacity and tensile strength of UHPFRC may be the reason why no fatigue damage initiated and propagated. This is why Test 10 lies just in the failure domain of the modified Goodman diagram, but did not fail. To grasp local variation of tensile resistance, an inverse analysis with stratification or randomization of material properties could be performed [51]

5. Conclusions

This paper presents the results of an experimental campaign on the fatigue resistance of fourteen full-size R-UHPFRC beams tested in four-point bending under both low and high minimum fatigue load levels. The following conclusions are drawn:

- The fatigue resistance of R-UHPFRC beams depends on both the minimum and maximum fatigue load level. The proposed modified Goodman diagram accordingly describes the fatigue resistance.
- Significant stress redistribution capacity takes place in the UHPFRC during fatigue loading influencing the stress range and thus the fatigue strength of steel reinforcement bars. The fatigue stress range in the rebar increases by 30% for Ø34 mm rebars and by 60% for Ø20 mm rebars, in the case of low minimum fatigue load ($F_{min} < 0.1S$). In the case of high minimum fatigue load ($F_{min} \approx 0.35S$), the corresponding stress increase is 10% for Ø34 mm rebars and 35% for Ø20 mm rebars. Thus, stress redistribution in the UHPFRC is less pronounced at higher stress level.

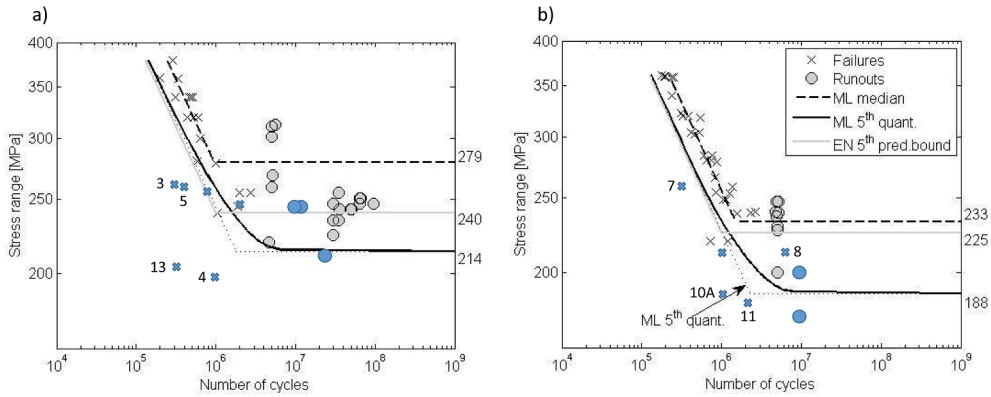

Fig. 4. Present test results (blue) projected on the S-N curves and results (grey) from [47] with rebar diameter a) ≤20 mm and b) >20 mm (ML – maximum likelihood fit, EN – Eurocode 5th quantile prediction bound). (For interpretation of the references to colour in this figure legend, the reader is referred to the web version of this article.)

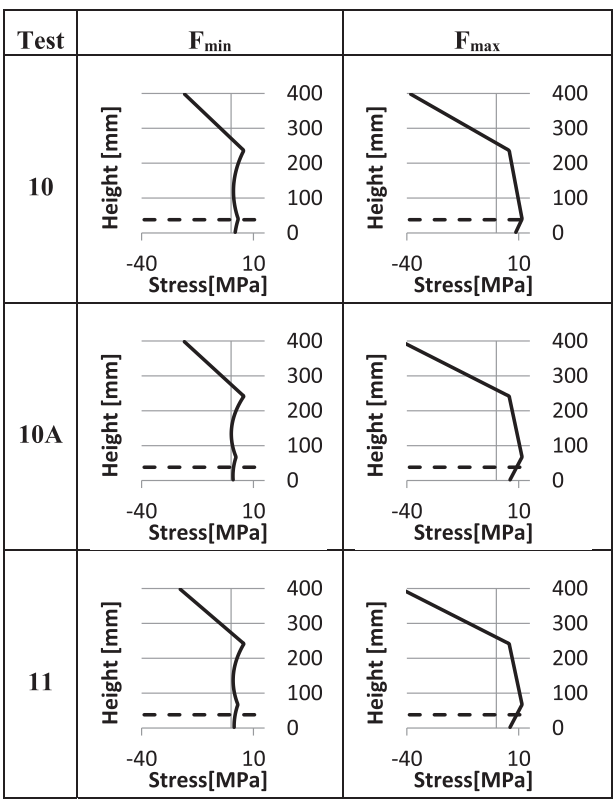

Fig. 5. Stress profile over the beam height in the UHPFRC for Tests 10, 10A and 11. The dashed line marks the position of the rebar.

- The fatigue resistance of R-UHPFRC beams shall be verified both 1) globally with respect to beam fatigue resistance using the modified Goodman diagram, and 2) locally with respect to the fatigue stress in the reinforcement bar considering stress increase due to UHPFRC – rebar interrelation.
- No fatigue failure occurs if 1) the normalized maximum and minimum loads lie within the safe region of the modified Goodman diagram; and 2) the stress range in the steel reinforcement bar, with increase due to stress redistribution taken into account, is below the Constant Amplitude Fatigue Limit of the given rebar.

Declaration of Competing Interest

The authors declare that they have no known competing financial interests or personal relationships that could have appeared to influence the work reported in this paper.

Acknowledgements

This project has received funding from the European Union's Horizon 2020 research and innovation program under the Marie Skłodowska-Curie grant agreement No 676139 – INFRASTAR.

Appendix A. Supplementary material

Supplementary data to this article can be found online at https://doi.org/10.1016/j.ijfatigue.2021.106216.

References

[1] Brühwiler E. Structural UHPFRC: Welcome to the post-concrete era. In: International Interactive Symposium on Ultra-High Performance Concrete, vol. 1. Des Moines, Iowa, USA: Iowa State University Digital Press; 2016. https://doi.org/10.21838/uhpc.2016.key.
[2] Graybeal B, Brühwiler E, Kim B-S, Toutlemonde F, Voo YL, Zaghi A. International Perspective on UHPC in Bridge Engineering. J Bridge Eng 2020;25:04020094. https://doi.org/10.1061/(ASCE)BE.1943-5592.0001630.
[3] Habel K, Denarié E, Brühwiler E. Experimental Investigation of Composite Ultra-High-Performance Fiber-Reinforced Concrete and Conventional Concrete Members. SJ 2007;104. https://doi.org/10.14359/18437.
[4] Lamothe S, Sorelli L, Blanchet P, Galimard P. Engineering ductile notch connections for composite floors made of laminated timber and high or ultra-high performance fiber reinforced concrete. Eng Struct 2020;211:110415. https://doi.org/10.1016/j.engstruct.2020.110415.
[5] Naaman AE. Fiber Reinforced Cement and Concrete Composites. 1st ed. Sarasota, Florida: Techno Press 3000; 2018.
[6] Resplendino J, Toutlemonde F. Designing and Building with UHPFRC. 1st ed. London: Wiley-ISTE; 2011.
[7] Spasojevic A, Redaelli D, Fernández Ruiz M, Muttoni A. Influence of tensile properties of UHPFRC on size effect in bending. Ultra High Performance Concrete (UHPC). In: Second International Symposium on Ultra High Performance Concrete, Kassel, Germany; 2008, p. 303–10.
[8] Brühwiler E, Friedl H, Rupp C, Escher H. Bau einer Bahnbrücke aus bewehrtem UHFB. Beton- Stahlbetonbau 2019;114:337–45. https://doi.org/10.1002/best.201900010.
[9] Lohaus L, Oneschkow N, Wefer M. Design model for the fatigue behaviour of normal-strength, high-strength and ultra-high-strength concrete. Struct Concr 2012;13:182–92. https://doi.org/10.1002/suco.201100054.
[10] FIB. Model Code 2010; 2010.
[11] Loraux C. Long-term monitoring of existing wind turbine towers and fatigue performance of UHPFRC under compressive stresses. Doctoral thesis. EPFL; 2018.
[12] SIA 2052. Technical Leaflet SIA 2052, UHPFRC - Materials, design and construction, Swiss Society of Engineers and Architects, Zurich; 2017.
[13] Herwig A. Reinforced concrete bridges under increased railway traffic loads. École polytechnique fédérale de Lausanne 2008.
[14] Schläfli M, Brühwiler E. Fatigue of Reinforced Concrete Elements without Shear Reinforcement. Lausanne, Switzerland: École Polytechnique Federale de Lausanne; 1998.
[15] Plos M, Gylltoft K, Lundgren K, Elfgren L, Cervenka J, Bruhwiler E, et al. Structural assessment of concrete railway bridges: Non-linear analysis and remaining fatigue life. In: Advances in Bridge Maintenance, Safety Management, and Life-Cycle

Performance, Set of Book & CD-ROM. CRC Press; 2006. p. 741–4. https://doi.org/10.1201/b18175-314.
[16] Mallett GP. Fatigue of reinforced concrete, vol. 2. London: HMSO; 1991.
[17] Hubbell D. Design and Development of Glass-Fibre-Reinforced Polymer and Ultra-High-Performance Fibre-Reinforced Concrete Guideway Girders. PhD Thesis. University of Toronto; 2017.
[18] Makita T, Brühwiler E. Tensile fatigue behaviour of ultra-high performance fibre reinforced concrete (UHPFRC). Mater Struct 2014;47:475–91. https://doi.org/10.1617/s11527-013-0073-x.
[19] Makita T, Brühwiler E. Tensile fatigue behaviour of Ultra-High Performance Fibre Reinforced Concrete combined with steel rebars (R-UHPFRC). Int J Fatigue 2014;59:145–52. https://doi.org/10.1016/j.ijfatigue.2013.09.004.
[20] Parant E, Rossi P, Boulay C. Fatigue behavior of a multi-scale cement composite. Cem Concr Res 2007;37:264–9. https://doi.org/10.1016/j.cemconres.2006.04.006.
[21] Lappa ES. High strength fibre reinforced concrete: Static and fatigue behaviour in bending. Delft University of Technology; 2007.
[22] Behloul M, Chanvillard G, Pimienta P, Pineaud A, Rivillon P. Fatigue Flexural Behavior of Pre-cracked Specimens of Special UHPFRC. SP 2005;228:1253–68.
[23] Farhat FA, Nicolaides D, Kanellopoulos A, Karihaloo BL. High performance fibre-reinforced cementitious composite (CARDIFRC) – Performance and application to retrofitting. Eng Fract Mech 2007;74:151–67. https://doi.org/10.1016/j.engfracmech.2006.01.023.
[24] Naaman AE, Hammoud H. Fatigue characteristics of high performance fiber-reinforced concrete. Cem Concr Compos 1998;20:353–63. https://doi.org/10.1016/S0958-9465(98)00004-3.
[25] Ríos JD, Cifuentes H. Probabilistic fatigue analysis of ultra-high-performance fibre-reinforced concrete under thermal effects. In: MATEC Web of Conferences, vol. 165; 2018. p. 12001. https://doi.org/10.1051/matecconf/201816512001.
[26] Carlesso DM, de la Fuente A, Cavalaro SHP. Fatigue of cracked high performance fiber reinforced concrete subjected to bending. Constr Build Mater 2019;220:444–55. https://doi.org/10.1016/j.conbuildmat.2019.06.038.
[27] Shen X, Brühwiler E. Biaxial flexural fatigue behavior of strain-hardening UHPFRC thin slab elements. Int J Fatigue 2020;138:105727. https://doi.org/10.1016/j.ijfatigue.2020.105727.
[28] Hoffman S, Weiher H. Innovative Design of Bridge Bearings by the use of UHPFRC. In: Proceedings of the 3rd International Symposium on UHPC and Nanotechnology for High Performance Construction Materials, Kassel, Germany. March 7, vol. 9; 2012. p. 973–80.
[29] Parsekian GA, Shrive NG, Brown TG, Kroman J, Perry V, Boucher A. Static and Fatigue Tests on Ductal® UHPFRC Footbridge Sections. SP 2008;253:273–90.
[30] Aaleti S, Sritharan S, Bierwagen D, Wipf T. Structural Behavior of Waffle Bridge Deck Panels and Connections of Precast Ultra-High-Performance Concrete. Transp Res Rec J Transp Res Board 2011;2251:82–92. https://doi.org/10.3141/2251-09.
[31] El-Hacha R, Abdelazeem H, Cariaga I. Performance of UHPC Crossarms for High-Voltage Transmission Lines. Designing and Building with UHPFRC. John Wiley & Sons, Ltd; 2013. p. 447–66. https://doi.org/10.1002/9781118557839.ch30.
[32] Sayed-Ahmed M, Sennah K. Ultimate and fatigue strength of GFRP-reinforced, full-depth, precast bridge deck panels with zigzag-shape transverse joints filled with UHPFRC, Vancouver, Canada; 2015.
[33] Graybeal B. Fatigue Response in Bridge Deck Connection Composed of Field-Cast Ultra-High-Performance Concrete. Transp Res Rec J Transp Res Board 2011;2251:93–100. https://doi.org/10.3141/2251-10.
[34] Makita T, Brühwiler E. Fatigue behaviour of bridge deck slab elements strengthened with reinforced UHPFRC. In: Proceedings Bridge Maintenance, Safety, Management, Resilience and Sustainability, vol. 1. Stresa, Italy: London, CRC Press/Balkema; 2012. p. 1974–80.
[35] Shao X, Qu W, Cao J, Yao Y. Static and fatigue properties of the steel-UHPC lightweight composite bridge deck with large U ribs. J Constr Steel Res 2018;148:491–507. https://doi.org/10.1016/j.jcsr.2018.05.011.
[36] Habel K, Viviani M, Denarié E, Brühwiler E. Development of the mechanical properties of an Ultra-High Performance Fiber Reinforced Concrete (UHPFRC). Cem Concr Res 2006;36:1362–70. https://doi.org/10.1016/j.cemconres.2006.03.009.
[37] SIA 262. Swiss standard SIA 262:2014 Concrete Structures; 2014.
[38] EC2. Eurocode 2: Design of concrete structures-Part 1-1: Genera rules and rules for buildings; 2005.
[39] Oneschkow N. Fatigue behaviour of high-strength concrete with respect to strain and stiffness. Int J Fatigue 2016;87:38–49. https://doi.org/10.1016/j.ijfatigue.2016.01.008.
[40] von der Haar C, Marx S. Development of stiffness and ultrasonic pulse velocity of fatigue loaded concrete. Struct Concr 2016;17:630–6. https://doi.org/10.1002/suco.201600007.
[41] Grünberg J, Lohaus L, Ertel C, Wefer M. Mehraxiales mechanisches Ermüdungsmodell von Ultra-Hochfestem Beton: Experimentelle und analytische Untersuchungen. Beton- Stahlbetonbau 2007;102:388–98. https://doi.org/10.1002/best.200700553.
[42] von der Haar C, Marx S. A strain model for fatigue-loaded concrete. Struct Concr 2017:1–9.
[43] Sawicki B, Brühwiler E, Denarié E. Inverse analysis of R-UHPFRC members to determine the flexural response underservice loading and at ultimate resistance. J Struct Eng; 2020 [Under review].
[44] Makita T, Brühwiler E. Modelling of fatigue behaviour of bridge deck slab elements strengthened with reinforced UHPFRC. In: Bridge Maintenance, Safety, Management and Life Extension, Shanghai, China. China: Boca Raton: CRC Press-Taylor & Francis Group; 2014. p. 2472–9.
[45] MacGregor JG, Jhamb IC, Nuttall N. Fatigue Strength of Hot Rolled Deformed Reinforcing Bars. JP 1971;68:169–79. https://doi.org/10.14359/11303.
[46] Oesterlee C. Structural Response of Reinforced UHPFRC and RC Composite Members. École polytechnique fédérale de Lausanne 2010.
[47] D'Angelo L, Rocha M, Nussbaumer A, Brühwiler E. S-N-P Fatigue Curves using Maximum Likelihood. In: Proceedings of 7th European Conference on Steel and Composite Structures, Naples, Italy: Brussels, ECCS European Convention for Constructional Steelwork; 2014. p. 705–6.
[48] Fisher JW, Viest IM. Fatigue tests of bridge materials of the AASHTO road test. Highway Research Board Special Report; 1961.
[49] Pfister JF, Hognestad E. High strength bars as concrete reinforcement, part 6: fatigue tests; 1964.
[50] Oesterlee C, Denarié E, Brühwiler E. Strength and deformability distribution in UHPFRC panels. Processing Sequence in the Production of Engineered Cementitious Composites 2009;1+2:390–7.
[51] Rossi P, Daviau-Desnoyers D, Tailhan J-L. Probabilistic numerical model of cracking in ultra-high performance fibre reinforced concrete (UHPFRC) beams subjected to shear loading. Cem Concr Compos 2018;90:119–25. https://doi.org/10.1016/j.cemconcomp.2018.03.019.